University of Reading

# *Kinetic multi-layer model of aerosol surface and bulk chemistry (KM-SUB): the influence of interfacial transport and bulk diffusion on the oxidation of oleic acid by ozone*

Article

Published Version

Shiraiwa, M., Pfrang, C. and Poschl, U. (2010) Kinetic multi-layer model of aerosol surface and bulk chemistry (KM-SUB): the influence of interfacial transport and bulk diffusion on the oxidation of oleic acid by ozone. Atmospheric Chemistry and Physics Discussions, 10 (1). pp. 281-326. ISSN 1680-7375 doi: 10.5194/acpd-10-281-2010 Available at https://centaur.reading.ac.uk/18018/

It is advisable to refer to the publisher's version if you intend to cite from the work. See Guidance on citing.

To link to this article DOI: http://dx.doi.org/10.5194/acpd-10-281-2010

Publisher: Copernicus Publications

All outputs in CentAUR are protected by Intellectual Property Rights law, including copyright law. Copyright and IPR is retained by the creators or other

University of Reading

copyright holders. Terms and conditions for use of this material are defined in the End User Agreement.

www.reading.ac.uk/centaur

**CentAUR**

Central Archive at the University of Reading

Reading's research outputs online

Atmos. Chem. Phys. Discuss., 10, 281–326, 2010
www.atmos-chem-phys-discuss.net/10/281/2010/
© Author(s) 2010. This work is distributed under
the Creative Commons Attribution 3.0 License.

Atmospheric Chemistry and Physics Discussions

This discussion paper is/has been under review for the journal Atmospheric Chemistry and Physics (ACP). Please refer to the corresponding final paper in ACP if available.

# Kinetic multi-layer model of aerosol surface and bulk chemistry (KM-SUB): the influence of interfacial transport and bulk diffusion on the oxidation of oleic acid by ozone

**M. Shiraiwa**[1], **C. Pfrang**[1,2], **and U. Pöschl**[1]

[1]Max Planck Institute for Chemistry, Biogeochemistry Department, P.O. Box 3060, 55128 Mainz, Germany
[2]University of Reading, Department of Chemistry, P.O. Box 224, Whiteknights, Reading RG6 6AD, UK

Received: 17 December 2009 – Accepted: 22 December 2009 – Published: 8 January 2010

Correspondence to: U. Pöschl (u.poschl@mpic.de)

Published by Copernicus Publications on behalf of the European Geosciences Union.



**Abstract**

We present a novel kinetic multi-layer model that explicitly resolves mass transport and chemical reaction at the surface and in the bulk of aerosol particles (KM-SUB). The model is based on the PRA framework of gas–particle interactions (Pöschl et al., 2007), and it includes reversible adsorption, surface reactions and surface-bulk exchange as well as bulk diffusion and reaction. Unlike earlier models, KM-SUB does not require simplifying assumptions about steady-state conditions and radial mixing. The temporal evolution and concentration profiles of volatile and non-volatile species at the gas-particle interface and in the particle bulk can be modeled along with surface concentrations and gas uptake coefficients.

In this study we explore and exemplify the effects of bulk diffusion on the rate of reactive gas uptake for a simple reference system, the ozonolysis of oleic acid particles, in comparison to experimental data and earlier model studies. We demonstrate how KM-SUB can be used to interpret and analyze experimental data from laboratory studies, and how the results can be extrapolated to atmospheric conditions. In particular, we show how interfacial transport and bulk transport, i.e., surface accommodation, bulk accommodation and bulk diffusion, influence the kinetics of the chemical reaction. Sensitivity studies suggest that in fine air particulate matter oleic acid and compounds with similar reactivity against ozone (C=C double bonds) can reach chemical lifetimes of multiple hours only if they are embedded in a (semi-)solid matrix with very low diffusion coefficients ($\leq 10^{-10}$ cm$^2$ s$^{-1}$).

Depending on the complexity of the investigated system, unlimited numbers of volatile and non-volatile species and chemical reactions can be flexibly added and treated with KM-SUB. We propose and intend to pursue the application of KM-SUB as a basis for the development of a detailed master mechanism of aerosol chemistry as well as for the derivation of simplified but realistic parameterizations for large-scale atmospheric and climate models.

## 1 Introduction

Aerosols are ubiquitous in the atmosphere and have strong effects on climate and public health (Seinfeld and Pandis 1998; Finlayson-Pitts and Pitts 2000; Pöschl, 2005). Depending on chemical composition and surface properties, aerosol particles can act as condensation nuclei for cloud droplets and ice crystals, and they can affect the abundance of trace gases through heterogeneous chemical reactions (Ammann et al., 1998; Pöschl, 2005; Fuzzi et al., 2006; Andreae and Rosenfeld, 2008; Hallquist et al., 2009). Gas-particle interactions can also significantly change the physical and chemical properties of aerosols such as toxicity, reactivity, hygroscopicity and radiative properties (Pöschl, 2002; Rudich, 2003; Kanakidou et al., 2005; Rincon et al., 2009; Wiedensohler et al., 2009). Chemical reactions and mass transport lead to continuous transformation and changes in the composition of atmospheric aerosols ("chemical aging") (Schwartz and Freiberg, 1981; Hanson, 1997; Smith et al., 2003; Ammann and Pöschl, 2007).

Atmospheric particles consist of a wide variety of organic and inorganic chemical compounds which can exist in different liquid or (semi-)solid states (crystalline, amorphous, glassy, ultraviscous, gel-like; Mikhailov et al., 2009). Chemical reactions can occur both at the surface and in the bulk of liquid and (semi-)solid particles. It is often difficult to discriminate surface and bulk reactions, and the relative importance of surface and bulk processes is not well understood (e.g., Moise and Rudich, 2000; Hearn et al., 2005; Pfrang et al., 2009).

Resistor model formulations are widely used to describe and investigate heterogeneous reactions and multiphase processes in laboratory, field and model studies of atmospheric chemistry (Hanson, 1997; Finlayson-Pitts and Pitts, 2000; Worsnop et al., 2002; Anttila et al., 2006; King et al., 2008, 2009; and references therein). The traditional resistor models, however, are usually based on simplifying assumptions such as steady state conditions, homogeneous mixing, and limited numbers of non-interacting species and processes.



In order to overcome these limitations, Pöschl, Rudich and Ammann have developed a kinetic model framework (PRA framework) with a double-layer surface concept and universally applicable rate equations and parameters for mass transport and chemical reactions at the gas-particle interface of aerosols and clouds (Pöschl et al., 2007). Ammann and Pöschl (2007) provided first examples on how the PRA framework can be applied to describe various physico-chemical processes in aerosols and clouds such as reactive gas uptake on solid particles and solubility saturation of liquid droplets under transient or steady-state conditions. Springmann et al. (2009) demonstrated the applicability and usefulness of the PRA framework in an urban plume box model of the degradation of benzo[a]pyrene on soot by ozone and nitrogen dioxide. Shiraiwa et al. (2009) presented a kinetic double-layer surface model (K2-SURF) and master mechanism for the degradation of a wide range of polycyclic aromatic hydrocarbons (PAHs) by multiple photo-oxidants ($O_3$, $NO_2$, OH and $NO_3$) through different types of parallel and sequential surface reactions. Pfrang et al. (2009) developed a kinetic double-layer model coupling aerosol surface and bulk chemistry (K2-SUB), in which mass transport and chemical reactions in the particle are not explicitly resolved but represented by a reacto-diffusive flux (Danckwerts, 1951; Hanson, 1997).

Here we present a kinetic-multi layer model of aerosol surface and bulk chemistry (KM-SUB) that explicitly treats all steps of mass transport and chemical reaction from the gas-particle interface to the particle core, resolving concentration gradients and diffusion throughout the particle bulk. We demonstrate the applicability of KM-SUB for a common model system of organic aerosol chemistry, the ozonolysis of oleic acid droplets, and we compare the results of our numerical simulations with the results of earlier experimental and theoretical studies of this system (Moise and Rudich, 2002; Katrib et al., 2004; King et al., 2004, 2009; Katrib et al., 2005; Ziemann, 2005; Hearn and Smith, 2007; Zahardis and Petrucci, 2007; Vesna et al., 2008; Pfrang et al., 2009; and references therein).

## 2 Model description

The kinetic multi-layer model of aerosol surface and bulk chemistry (KM-SUB) builds on the formalism and terminology of the PRA framework (Pöschl et al., 2007). A list of symbols is given in Appendix A.

As illustrated in Fig. 1, KM-SUB consists of multiple model compartments and layers, respectively: gas phase, near-gas phase, sorption layer, quasi-static surface layer, near-surface bulk, and a number of $n$ bulk layers. The quasi-static surface layer has a monolayer thickness that corresponds to the (average) effective molecular diameter of non-volatile species $Y_j$ ($\delta_{Y_j}$). The thickness of bulk layer ($\delta$) follows from the number of layers ($n$) and particle radius ($r_p$): $\delta=(r_p-\delta_{Y_j})/n$.

The following processes are considered in KM-SUB: gas phase diffusion, gas-surface transport (reversible adsorption), surface layer reactions, surface-bulk transport, bulk diffusion, and bulk reactions. As outlined in the PRA framework, the following differential equations can be used to describe the mass balance of volatile species $X_i$ and non-volatile species $Y_j$ for each model layer:

$$\mathrm{d}[X_i]_s/\mathrm{d}t = J_{\mathrm{ads},X_i} - J_{\mathrm{des},X_i} + P_{s,X_i} - L_{s,X_i} - J_{s,b,X_i} + J_{b,s,X_i} \quad (1)$$

$$\mathrm{d}[Y_j]_{ss}/\mathrm{d}t = J_{b,ss,Y_j} - J_{ss,b,Y_j} + P_{ss,Y_j} - L_{ss,Y_j} \quad (2)$$

$$\mathrm{d}[X_i]_{b1}/\mathrm{d}t = (J_{s,b,X_i} - J_{b,s,X_i})A(1)/V(1) - (J_{b1,b2,X_i} - J_{b2,b1,X_i})A(2)/V(1) + P_{b1,X_i} - L_{b1,X_i} \quad (3)$$

$$\mathrm{d}[Y_j]_{b1}/\mathrm{d}t = (J_{ss,b,Y_j} - J_{b,ss,Y_j})A(1)/V(1) - (J_{b1,b2,Y_j} - J_{b2,b1,Y_j})A(2)/V(1) + P_{b1,Y_j} - L_{b1,Y_j} \quad (4)$$

$$\mathrm{d}[X_i]_{bk}/\mathrm{d}t = (J_{bk-1,bk,X_i} - J_{bk,bk-1,X_i})A(k)/V(k) - (J_{bk,bk+1,X_i} - J_{bk+1,bk,X_i})A(k+1)/V(k) + P_{bk,X_i} - L_{bk,X_i} \quad (k=2,\ldots,n-1) \quad (5)$$



$$\mathrm{d}[Y_j]_{bk}/\mathrm{d}t = (J_{bk-1,bk,Y_j} - J_{bk,bk-1,Y_j})A(k)/V(k) - (J_{bk,bk+1,Y_j} - J_{bk+1,bk,Y_j})A(k+1)/V(k) + P_{bk,Y_j} - L_{bk,Y_j} \quad (k=2,\ldots,n-1) \quad (6)$$

$$\mathrm{d}[X_i]_{bn}/\mathrm{d}t = (J_{bn-1,bn,X_i} - J_{bn,bn-1,X_i})A(n)/V(n) + P_{bn,X_i} - L_{bn,X_i} \quad (7)$$

$$\mathrm{d}[Y_j]_{bn}/\mathrm{d}t = (J_{bn-1,bn,Y_j} - J_{bn,bn-1,Y_j})A(n)/V(n) + P_{bn,Y_j} - L_{bn,Y_j} \quad (8)$$

The various types of mass transport fluxes ($J$) and rates of chemical production and loss ($P$, $L$) are defined in the list of symbols (Appendix A). $A(k)$ and $V(k)$ are the outer surface area and the volume of the bulk layer $k$, respectively (Fig. 1). For spherical particles, $A(k)$ and $V(k)$ can be calculated from the particle bulk radius ($r_b=r_p-\delta_{Y_j}$), bulk layer thickness ($\delta$) and layer index number $k$ as follows.

$$V(k) = \frac{4}{3}\pi\left[(r_b-(k-1)\delta)^3 - (r_b-k\delta)^3\right] \quad (9)$$

$$A(k) = 4\pi(r_b-(k-1)\delta)^2 \quad (10)$$

For planar geometry (thin films), the surface-to-volume ratio is constant:

$$A(k)/V(k) = 1/\delta \quad (11)$$

The surface-to-volume ratios of the layers play an important role in accounting for particle geometry. The absolute number of non-volatile molecules $Y_j$ in the particle ($N_{Y_j}$) can be calculated as follows:

$$N_{Y_j} = [Y_j]_{ss}A_{ss} + \sum_{k=1}^{n}[Y_j]_{bk}V(k) \quad (12)$$

where $A_{ss}$ is the surface area of the particle. In the following sub-sections we specify the formalisms used to describe and calculate fluxes or rates of gas-surface interactions, surface-bulk transport, bulk diffusion and bulk reactions.

### 2.1 Gas-surface interactions and surface layer reactions

The principles and details of gas-phase and gas-surface transport ($J_{ads}$, $J_{des}$) and surface layer reactions ($L_s$, $L_{ss}$, $P_s$, $P_{ss}$) have been discussed and illustrated in the PRA framework (Pöschl et al., 2007; Ammann and Pöschl, 2007) and in the K2-SURF study of aerosol surface chemistry (Shiraiwa et al., 2009). Here we just briefly summarize the key aspects and equations. The fluxes of surface collisions, adsorption and desorption of a volatile species $X_i$ ($J_{coll,X_i}$, $J_{ads,X_i}$ and $J_{des,X_i}$) are given by:

$$J_{coll,X_i} = [X_i]_{gs}\omega_{X_i}/4 \tag{13}$$

$$J_{ads,X_i} = \alpha_{s,X_i} J_{coll,X_i} \tag{14}$$

$$J_{des,X_i} = k_{d,X_i}[X_i]_s \tag{15}$$

$$\alpha_{s,X_i} = \alpha_{s,0,X_i}(1-\theta_s) \tag{16}$$

$$\theta_s = \sum_i \sigma_{s,X_i}[X_i]_s \tag{17}$$

$[X_i]_{gs}$ is the near-surface gas phase concentration of $X_i$, $\omega_{X_i}$ is the mean thermal velocity, $\alpha_{s,X_i}$ is the surface accommodation coefficient, and $k_{d,X_i}$ is the desorption rate coefficient or inverse desorption lifetime, respectively $\left(k_{d,X_i}=\tau_{d,X_i}^{-1}\right)$. $\alpha_{s,0,X_i}$ is the surface accommodation coefficient on an adsorbate-free surface, $\sigma_{s,X_i}$ is the effective molecular cross section of $X_i$ in the sorption layer, and $\theta_s$ is the surface coverage by adsorbed species.

For slow gas uptake and in the gas kinetic-regime (small uptake coefficient, large Knudsen number), $[X_i]_{gs}$ is practically the same as the average gas phase concentration of $X_i$ in the investigated system, $[X_i]_g$. For rapid gas uptake in the continuum or transition regime (large uptake coefficient, small Knudsen number), the gas phase diffusion correction factor $C_{g,X_i}$ can be used to calculate $[X_i]_{gs}$ from $[X_i]_g$: $[X_i]_{gs}=C_{g,X_i}[X_i]_g$



(Pöschl et al., 2007; Shiraiwa et al., 2009). The uptake coefficient ($\gamma_{X_i}$) for $X_i$ is given by:

$$\gamma_{X_i} = \frac{J_{ads,X_i} - J_{des,X_i}}{J_{coll,X_i}} + \gamma_{gsr,X_i} \tag{18}$$

$\gamma_{gsr,X_i}$ is the reaction probability for elementary gas-surface reactions (potentially relevant for free radicals but assumed to be zero in the remainder of this study.

General rate equations of chemical production and loss by surface layer reactions ($P_{s,X_i}$, $P_{ss,Y_i}$, $L_{s,X_i}$, $L_{ss,Y_i}$) are specified in the PRA framework (Sect. 3.3, Pöschl et al., 2007). Different types of surface layer reactions can proceed within the sorption layer ($P_{s,s,X_i}-L_{s,s,X_i}$), within the quasi-static surface layer ($P_{ss,ss,Y_j}-L_{ss,ss,Y_j}$), and between sorption layer and quasi-static layer ($P_{s,ss,X_i}-L_{s,ss,X_i}$, $P_{ss,s,Y_j}-L_{ss,s,Y_j}$). The generalized rate equations for reactions between volatile species $X_i$ in the sorption layer and non-volatile species $Y_j$ in the quasi-static layer are given by:

$$P_{s,ss,X_i} - L_{s,ss,X_i} = \sum_v \sum_p \sum_q c_{SLRv,s,X_i} k_{SLRv,X_p,Y_q}[X_p]_s[Y_q]_{ss} \tag{19}$$

$$P_{ss,ss,Y_j} - L_{ss,ss,Y_j} = \sum_v \sum_p \sum_q c_{SLRv,ss,Y_j} k_{SLRv,X_p,Y_q}[X_p]_s[Y_q]_{ss} \tag{20}$$

Here $c_{SLRv,s,X_i}$ and $c_{SLRv,ss,Y_j}$ stand for the stoichiometric coefficients (negative for starting materials and positive for reaction products) of species $X_i$ and $Y_j$ in reaction SLR$v$; $v=1,\ldots,v_{max}$ in a system with a total number of $v_{max}$ (photo-)chemical reactions occurring on the surface of the investigated aerosol particles. $k_{SLRv,X_p,Y_q}$ is a second-order reaction rate coefficient. In the exemplary simulations of the ozonolysis of oleic acid performed in this study and presented in Sect. 3, we consider only chemical loss and a second-order surface layer reaction between $O_3$ (X) and oleic acid (Y) with the following rate equation:

$$L_{s,X} = L_{ss,Y} = k_{SLR,X,Y}[X]_s[Y]_{ss} \tag{21}$$

### 2.2 Surface-bulk transport

The surface-bulk transport of volatile species $X_i$ ($J_{s,b,X_i}$ and $J_{b,s,X_i}$) is defined as exchange between sorption layer and near-surface bulk, and the surface–bulk transport of non-volatile species $Y_j$ ($J_{ss,b,Y_j}$ and $J_{b,ss,Y_j}$) is defined as exchange between quasi-static surface layer and near-surface bulk. Based on the PRA framework, surface to bulk transport can be described by:

$$J_{s,b,X_i} = k_{s,b,X_i}[X_i]_s \tag{22}$$

$$J_{ss,b,Y_j} = k_{ss,b,X_j}[Y_j]_{ss} \tag{23}$$

$k_{s,b,X_i}$ and $k_{ss,b,Y_j}$ are first-order transport rate coefficients ($s^{-1}$) of $X_i$ and $Y_j$, respectively. In the same way, bulk to surface transport ($J_{b,s,X_i}$ and $J_{b,ss,Y_j}$) can be described as follows:

$$J_{b,s,X_i} = k_{b,s,X_i}[X_i]_{b1} \tag{24}$$

$$J_{b,ss,Y_j} = k_{b,ss,X_j}[Y_j]_{b1} \tag{25}$$

$k_{b,s,X_i}$ and $k_{b,ss,Y_j}$ ($cm\,s^{-1}$) are transport rate coefficients, which can be regarded as effective transport velocities. Estimates for these effective transport velocities can be derived from the corresponding bulk diffusion coefficients $D_{b,X_i}$ and $D_{b,Y_j}$ ($cm^2\,s^{-1}$) by considering the average distance traveled by molecules diffusing in one direction: $x=(4D_b t/\pi)^{1/2}$ (Atkins, 1998; Pfrang et al., 2009). On average, a molecule $Y_j$ in the near-surface bulk layer ($k=1$) needs to travel a distance of $x\approx(\delta+\delta_{Y_j})/2$ to move into the quasi-static surface layer. The average time required to travel over this distance by diffusion is $t=(\delta+\delta_{Y_j})^2\pi/(16D_{b,Y_j})$. By division of travel distance over travel time we obtain the following estimate for the effective transport velocity:

$$k_{b,ss,Y_j} \approx 8D_{b,Y_j}/((\delta+\delta_{Y_j})\pi) \tag{26}$$



For pure $Y_j$ under equilibrium conditions, mass conservation implies $k_{b,ss,Y_j}[Y_j]_{b1} = k_{ss,b,Y_j}[Y_j]_{ss}$, and the surface and bulk concentrations are given by the inverse of the effective molecular cross section and of the effective molecular volume, respectively: $[Y_i]_{ss}=\delta_{Y_j}^{-2}$ and $[Y_i]_{b1}=\delta_{Y_j}^{-3}$. Thus, we obtain

$$k_{ss,b,Y_j} \approx k_{b,ss,Y_j}/\delta_{Y_j} \approx 8D_{b,Y_j}/((\delta+\delta_{Y_j})\delta_{Y_j}\pi) \tag{27}$$

In analogy, the bulk-to-surface transport velocity of $X_i$ can be calculated for an average travel distance of $x\approx(\delta+\delta_{X_i}+2\delta_{Y_j})/2$ from the near-surface bulk layer into the sorption layer:

$$k_{b,s,X_i} \approx 8D_{b,X_i}/((\delta+\delta_{X_i}+2\delta_{Y_j})\pi) \tag{28}$$

An estimate for $k_{s,b,X_i}$ can be determined by matching the rate coefficients for gas-surface and surface-bulk transport with a literature value or estimate for the gas-particle equilibrium partitioning coefficient ($K_{sol,cc,X_i}$) or Henry's law coefficient, respectively (Pöschl et al., 2007):

$$k_{s,b,X_i} = \frac{4k_{b,s,X_i}K_{sol,cc,X_i}k_{d,X_i}}{\alpha_{s,X_i}\omega_{X_i}} \tag{29}$$

where $k_{d,X_i}$ is the first-order rate coefficient of desorption. From the fluxes and rates of gas-surface transport, surface-bulk transport and surface reaction follows the bulk accomodation coefficient of $X_i$:

$$\alpha_{b,X_i} = \alpha_{s,X_i}\frac{J_{s,b,X_i}}{J_{des,X_i}+J_{s,b,X_i}+L_{s,X_i}} \tag{30}$$

### 2.3 Bulk diffusion

Bulk diffusion is explicitly treated in the KM-SUB model as the mass transport ($J_{bk,bk+1}$) from one bulk layer (bulk $k$) to the next (bulk $k+1$). In analogy to surface–bulk mass

transport, we describe the mass transport fluxes between different layers of the bulk by first-order rate equations:

$$J_{\mathrm{b}k,\mathrm{b}k+1,\mathrm{X}_i} = k_{\mathrm{b,b,X}_i}[\mathrm{X}_i]_{\mathrm{b}k} \tag{31}$$

$$J_{\mathrm{b}k,\mathrm{b}k+1,\mathrm{Y}_j} = k_{\mathrm{b,b,Y}_j}[\mathrm{Y}_j]_{\mathrm{b}k} \tag{32}$$

Estimates for the transport rate coefficients or effective velocities of $\mathrm{X}_i$ and $\mathrm{Y}_j$, $k_{\mathrm{b,b,X}_i}$ and $k_{\mathrm{b,b,Y}_j}$ ($\mathrm{cm\,s^{-1}}$), can be calculated from the corresponding diffusion coefficients. For this purpose we assume that each layer is homogeneously mixed (no concentration gradient within a layer) and that the average travel distance for molecules moving from one layer to the next is the layer thickness $\delta$:

$$k_{\mathrm{b,b,X}_i} = 4D_{\mathrm{b,X}_i}/(\pi\delta) \tag{33}$$

$$k_{\mathrm{b,b,Y}_j} = 4D_{\mathrm{b,Y}_j}/(\pi\delta) \tag{34}$$

This treatment of bulk diffusion yields practically the same results (concentration profiles) as the solving of partial differential equations (Smith et al. 2003), but it is more flexible and requires no assumptions about interfacial transport. As detailed in Appendix B, the ozone concentrations calculated for the near-surface bulk indicate that the assumption of Henry's law equilibrium is not a realistic boundary layer condition for the PDE method when applied to reactive systems.

### 2.4 Bulk reaction

Chemical reactions proceeding within the bulk of a particle are defined as bulk reactions (BR). For simplicity, we assume that all relevant bulk reactions proceed via quasi-elementary steps with straightforward first- or second-order rate dependences on the concentrations within each bulk layer. The following generalized expressions



can be used to describe net chemical production (i.e. production minus loss) of bulk species $\mathrm{X}_i$ or $\mathrm{Y}_j$ within the bulk layer $k$.

$$P_{\mathrm{b}k,\mathrm{X}_i} - L_{\mathrm{b}k,\mathrm{X}_i} = \sum_v \sum_p c_{\mathrm{BR}v,\mathrm{X}_i}[\mathrm{X}_p]_{\mathrm{b}k} \left(k_{\mathrm{BR}v,\mathrm{X}_p} + \sum_q k_{\mathrm{BR}v,\mathrm{X}_p,\mathrm{X}_q}[\mathrm{X}_q]_{\mathrm{b}k} + \sum_r k_{\mathrm{BR}v,\mathrm{X}_p,\mathrm{Y}_r}[\mathrm{Y}_r]_{\mathrm{b}k}\right) \tag{35}$$

$$P_{\mathrm{b}k,\mathrm{Y}_i} - L_{\mathrm{b}k,\mathrm{Y}_i} = \sum_v \sum_p c_{\mathrm{BR}v,\mathrm{Y}_i}[\mathrm{Y}_p]_{\mathrm{b}k} \left(k_{\mathrm{BR}v,\mathrm{Y}_p} + \sum_q k_{\mathrm{BR}v,\mathrm{Y}_p,\mathrm{Y}_q}[\mathrm{Y}_q]_{\mathrm{b}k} + \sum_r k_{\mathrm{BR}v,\mathrm{X}_r,\mathrm{Y}_p}[\mathrm{X}_r]_{\mathrm{b}k}\right) \tag{36}$$

Here $c_{\mathrm{BR}v,\mathrm{X}_i}$ and $c_{\mathrm{BR}v,\mathrm{Y}_j}$ stand for the stoichiometric coefficients (negative for starting materials and positive for reaction products) of species $\mathrm{X}_i$ and $\mathrm{Y}_j$ in reaction BR$v$; $v$=1,...,$v_{\max}$ in a system with a total number of $v_{\max}$ chemical reactions occurring in the bulk layer $k$. $k_{\mathrm{BR}v,\mathrm{X}_p}$ and $k_{\mathrm{BR}v,\mathrm{Y}_p}$ are first-order reaction rate coefficients and $k_{\mathrm{BR}v,\mathrm{X}_p,\mathrm{X}_q}$, $k_{\mathrm{BR}v,\mathrm{X}_p,\mathrm{Y}_r}$ and $k_{\mathrm{BR}v,\mathrm{Y}_p,\mathrm{Y}_q}$ are second-order reaction rate coefficients. In principle, higher-order reactions might also occur in real systems and could be flexibly included in the model. In the exemplary simulations of the ozonolysis of oleic acid performed in this study and presented in Sect. 3, we consider only chemical loss and a second-order bulk reaction between $\mathrm{O_3}$ (X) and oleic acid (Y) with the following rate equation:

$$L_{\mathrm{b}k,\mathrm{X}} = L_{\mathrm{b}k,\mathrm{Y}} = k_{\mathrm{BR,X,Y}}[\mathrm{X}]_{\mathrm{b}k}[\mathrm{Y}]_{\mathrm{b}k} \tag{37}$$

## 3 Model application: oxidation of oleic acid by ozone

To test and demonstrate the applicability of the KM-SUB model, we have simulated the oxidation of oleic acid particles by ozone in comparison to experimental data from

Ziemann (2005). The same data set has recently been used by Pfrang et al. (2009) for simulations with a kinetic double-layer model (K2-SUB). The gas phase ozone concentration was set to $[X]_g=[X]_{gs}=7.0\times10^{13}$ cm$^{-3}$ (corresponding to 2.8 ppm at 1013 hPa and 298 K). The initial surface and bulk concentrations of ozone (X) were set to $[X]_{s,0}=[X]_{bk,0}=0$, and the initial surface and bulk concentrations of oleic acid (Y) were set to $[Y]_{ss,0}=9.7\times10^{13}$ cm$^{-2}$ and $[Y]_{ss,0}=1.2\times10^{21}$ cm$^{-3}$, respectively. Accordingly, the initial value of the total number of oleic acid molecules in particles with a radius of 0.2 µm was $N_{Y,0}=4.1\times10^{7}$.

We modeled the temporal evolution of the particle surface and bulk composition and of the ozone uptake coefficient by numerically solving the differential equations of mass balance for each model compartment (Eqs. 1–8) with Matlab software (ode23tb solver with 999 time steps). The kinetic parameters required for the model simulations are summarized in Table 1: the surface accommodation coefficient of ozone ($\alpha_{s,0,X}$), the desorption lifetime of ozone ($\tau_{d,X}$), the bulk diffusion coefficients of ozone and oleic acid ($D_{b,X}$, $D_{b,Y}$), the second-order surface layer reaction rate coefficient ($k_{SLR,X,Y}$), and the second-order bulk reaction rate coefficient ($k_{BR,X,Y}$). Additional input parameters were the mean thermal velocity of ozone ($\omega_X=3.6\times10^{4}$ cm s$^{-1}$) and the molecular diameters of oleic acid ($\delta_Y=0.8$ nm) and ozone ($\delta_X=0.4$ nm).

We have investigated three different model scenarios (base cases) to characterize the influence of different parameters and conditions on the uptake of ozone and the decay of oleic acid. In base case 1 (BC1) we assume fast bulk reaction leading to kinetic limitation by interfacial transport. In base case 2 (BC2) we assume slow bulk reaction (kinetic limitation by bulk reaction) and in base case 3 (BC3) we assume slow bulk diffusion (kinetic limitation by bulk diffusion). Unless mentioned otherwise, the simulations were performed with $n=100$ layers corresponding to a layer thickness of $\delta=1.99$ nm for $r_p=0.2$ µm.



### 3.1 Base case 1: kinetic limitation by interfacial transport

Figure 2 illustrates the model results of KM-SUB in base case 1 with the kinetic parameters specified in Table 1. As shown in Fig. 2a, the simulated decay of oleic acid is in very good agreement with the experimentally observed decay. Throughout the experimental time scale of 1–15 s, the simulated ozone uptake coefficient is nearly constant and identical to the surface and bulk accommodation coefficients ($\gamma_X\approx\alpha_{b,X}\approx\alpha_{s,X}\approx\alpha_{s,0,X}\approx4\times10^{-4}$), indicating that the gas uptake is limited by interfacial mass transport, i.e., by the process of bulk accommodation which is in turn limited by the process of surface accommodation. After ~30 s the ozone uptake coefficient rapidly drops off when reaction partner oleic acid is used up by the rapid bulk reaction ($\gamma_X/\gamma_{X,0}\approx N_Y/N_{Y,0}<1\%$ after ~37 s).

As shown in Fig. 2b, the surface concentration of oleic acid also decreases gradually over the first ~30 s and drops off rapidly afterwards. In contrast, the surface concentration of ozone exhibits a rapid initial increase from zero to a plateau level of $[X]_s\approx10^{11}$ cm$^{-2}$, which is reached within less than a second (~20 ms) and determined by the combination of reversible adsorption, surface reaction, and surface-to-bulk transport driven by the chemical reaction in the bulk. Over the first 30 s, $[X]_s$ gradually increases with the decay of oleic acid and the related decrease of chemical loss. As the chemical loss by reaction with oleic acid rapidly drops off after ~30 s, $[X]_s$ swiftly increases by an order of magnitude to a steady-state-level of $\sim10^{12}$ cm$^{-2}$, which is governed by reversible adsorption.

To test how the number of model layers in the particle bulk affects the simulation results, we have run the model with $n=1$, 5 and 100 layers corresponding to layer thicknesses of $\delta=199.2$, 39.8 and 1.99 nm, respectively. The results obtained with $n=100$ and 5 were practically identical, demonstrating the robustness of the multi-layer model approach with transport rate coefficients (velocities) scaled by the layer thickness (Eqs. 28–31). As shown in Fig. 2, the deviations obtained with $n=1$ were relatively minor, but they indicate that the particle bulk cannot be regarded as well mixed

under the conditions of base case 1. Similar deviations were obtained with the kinetic double-layer model K2-SUB, in which the bulk processes are not explicitly resolved but represented by a reacto-diffusive flux (Appendix C, Pfrang et al., 2009).

The KM-SUB model results for the bulk concentration profiles of ozone and oleic acid were also essentially the same with $n$=100 and 5. For high resolution and to avoid congestion of the plot, however, only the profiles obtained 100 layers are shown in Fig. 3. The $y$-axis indicates the radial distance from the particle center ($r$) normalized by the particle radius ($r_p$), ranging from the particle core ($\delta/r_p \approx 0$) to the near-surface bulk ($(r_p - \delta)/r_p \approx 1$).

As shown in Fig. 3a, ozone rapidly diffuses into the particle bulk. A gradient between the near-surface bulk and the core is established within less than a second (~20 ms), and the concentration profile is determined by the interplay of interfacial mass transport (surface and bulk accommodation) with bulk diffusion and chemical reaction. During the first few seconds, the ozone concentration in the particle core is about a factor of ~50 lower than in the near surface bulk. Up to ~30 s, the ozone concentration gradient decreases gradually with the decay of oleic acid and the related decrease of chemical loss. As the chemical loss by reaction with oleic acid rapidly drops off after ~30 s, the ozone concentration gradient swiftly relaxes, and after ~37 s ozone is well mixed throughout the particle bulk at the concentration level of solubility saturation ($[X]_{b,sat} = 8\times10^{14}\ cm^{-3} = K_{sol,CC,X}[X]_{gs}$ with $K_{sol,CC,X} = 4.8\times10^{-4}\ mol\,cm^{-3}\,atm^{-1}$).

As shown in Fig. 3b, the ozone gradient and the ozonolysis of oleic acid cause a reverse gradient in the bulk concentration of oleic acid. Because the concentration of oleic acid is several orders of magnitude larger than that of ozone, however, the strong gradient of ozone induces only a small gradient in oleic acid. During the first few seconds, the oleic acid concentration in the near-surface bulk is ~5% lower than in the particle core. As the ozone gradient relaxes after ~30 s, the small oleic acid gradient also disappears. Thus, oleic acid can effectively be regarded as well-mixed.

Figure 4a shows the loss rate of oleic acid and ozone by chemical reaction in the particle bulk ($L_b$) as calculated with KM-SUB for different model layers and with KM-SUB



and K2-SUB effectively averaged over the whole bulk volume. The averaged values of $L_b$ calculated by K2-SUB and KM-SUB are almost identical, demonstrating consistency of KM-SUB with K2-SUB and with the underlying resistor model formulation of the reacto-diffusive flux $J_{b,rd}$. Due to the overall kinetic limitation by interfacial transport, the volume-average loss rate $L_b$ remains near-constant up to ~30 s. During the first few seconds, the loss rate in the near-surface bulk ($L_{b1}$, $r/r_p \approx 1$) is more than a factor of 2 higher than the volume-average loss rate, while the loss rates in layers around the particle core ($L_{b40}$ to $L_{b100}$, $r/r_p < 0.6$) are more than a factor of 2 lower. $L_{b1}$ continually decreases due to progressing consumption of oleic acid, whereas $L_{b40}$ to $L_{b100}$ exhibit a pronounced increase up to ~35 s due to the penetration of ozone to the particle core (see also Fig. 3a). After ~35 s all loss rates drop off rapidly and approach zero after ~37 s as oleic acid is essentially used up.

Up to ~30 s, the strong radial gradient of loss rates $L_b$ and the approximate coincidence of $L_{b20}$ ($r/r_p \approx 0.8$) with $L_b$ indicate that the overall rate of conversion or absolute loss rate of oleic acid and ozone molecules in the particle is strongly dominated by the outer bulk layers at $r/r_p > 0.8$. Due to the spherical geometry the outer layers also have much larger volumes, which further enhances their relative importance with regard to the absolute loss rate of molecules in each layer ($L^*_{bk} = L_{bk}V_{bk}$) and in the entire particle ($L^*_b = L_bV_b$). Figure 4b illustrates this by displaying the values of $L^*_{bk}$ and $L^*_b$ corresponding to the values of $L_{bk}$ and $L_b$ displayed in Fig. 4a (note the linear scaling of Fig. 4a and the logarithmic scaling of Fig. 4b). $L^*_b$ calculated by KM-SUB and K2-SUB are almost identical.

The black solid line in Fig. 3a represents the reacto-diffusive length for ozone normalized by the particle radius ($1 - l_{rd}/r_p$), which can be regarded as the distance from the surface up to which the chemical reaction proceeds effectively (Finlayson-Pitts and Pitts, 2000; Pöschl et al., 2007). The initial value of $l_{rd,X} \approx 20$ nm is consistent with the values reported by Smith et al. (2003) and Katrib et al. (2004). Over the first ~30 s of the model run $l_{rd,X}$ remains fairly constant, and the reacto-diffusive line (black solid) coincides with the 50% isoline for the concentration difference between the particle

core and the near-surface bulk (black dotted), and with the 63% (=1 – 1/e) isoline of $L_b^*$ (black dashed). During this time 63% of $L_b^*$, i.e., 63% of the overall rate of conversion of oleic acid ozonolysis, occur in the outermost 10 bulk layers, i.e. at $r/r_p$>0.9 (corresponding to ~30% of the particle bulk volume). After ~30 s, $l_{rd,X}$ increases steeply as oleic acid is depleted and ozone can freely penetrate throughout the bulk of the particle.

### 3.2 Base case 2: kinetic limitation by bulk reaction

In base case 2 the second-order bulk reaction rate coefficient was by a factor of ~30 smaller than in BC1, while the surface accommodation coefficient was by a factor of ~2 higher (Table 1).

As shown in Fig. 5a, the simulation results of BC2 are also in very good agreement with the observed decay of oleic acid. The calculated ozone uptake coefficient, however, behaves very differently than in BC1. The initial value of $\gamma_X$ in BC2 is by a factor of ~2 higher than in BC1. It reflects rapid uptake into the initially ozone-free particle bulk, which is limited by the kinetics of interfacial transport, i.e., bulk accommodation and surface accommodation, respectively. After less than one second (~20 ms), however, $\gamma_X$ steeply drops off to a level that is reaction-limited ($\gamma_X \approx 10^{-4} < \alpha_{b,X} \approx 8\times10^{-4}$) and continues to decrease gradually with decreasing abundance of the reaction partner oleic acid.

After a rapid initial increase (~20 ms), the ozone surface concentration reaches a plateau level which increases only slightly until the end of the simulation, while the oleic acid surface concentration decreases gradually. In contrast to BC1, none of the compositional and kinetic parameters exhibit abrupt changes after ~30 s. Instead, they all undergo a gradual evolution reflecting the kinetics of the rate-limiting bulk reaction.

The results of multi-layer model KM-SUB with both $n$=100 and 1 were practically identical to the results of the double-layer model K2-SUB, indicating that the particle bulk can be regarded as well mixed under the conditions of BC 2.

Due to faster interfacial transport and slower chemical reaction, the ozone concen-



tration in the bulk increases much faster than in BC1 (Fig. 6a vs. Fig. 3a). After less than one second (~20 ms), the ozone concentration in the core of the particle is only ~30% lower than in the near-surface bulk, and the gradient continues to decrease with decreasing abundance of oleic acid. Due to the slow decay of oleic acid, however, a small ozone gradient persists until the end of the simulation (Fig. 6a) and thus longer than in BC1, where the initially very strong gradient essentially disappears after ~37 s when practically all oleic acid (>99%) has been consumed by the rapid bulk reaction (Fig. 3a). As illustrated in Fig. 6b, oleic acid can be regarded as well-mixed (concentration differences <1%).

Figure 7a shows the loss rate of oleic acid and ozone by chemical reaction in the particle bulk ($L_b$) as calculated with KM-SUB for different model layers and with KM-SUB and K2-SUB effectively averaged over the whole bulk volume. The average values of $L_b$ calculated by K2-SUB and KM-SUB are almost identical. Due to the kinetic limitation by bulk reaction, the volume-average loss rate $L_b$ decreases continuously due to consumption of oleic acid. Initially, $L_b$ in the near-surface bulk ($L_{b1}$, $r/r_p \approx 1$) is ~40% higher than that in the core ($L_{b100}$) corresponding to the concentration gradient of $O_3$ in the bulk. They become almost same in 20 s as concentration gradient becomes smaller. Figure 7b illustrates $L_{bk}^*$ (=$L_{bk}V_{bk}$) and $L_b^*$ (=$L_bV_b$) corresponding to the values of $L_{bk}$ and $L_b$ displayed in Fig. 7a (note the linear scaling of Fig. 7a and the logarithmic scaling of Fig. 7b). $L_b^*$ calculated by KM-SUB and K2-SUB are almost identical.

The black solid line in Fig. 6a represents again the reacto-diffusive length for ozone normalized by the particle radius ($1 - l_{rd}/r_p$). Due to the lower reaction rate coefficient, the initial value of $l_{rd,X} \approx 120$ nm is by a factor of ~6 larger than in BC1, and after ~20 s it is already larger than the particle radius (200 nm), indicating that the reaction effectively proceeds throughout the whole bulk. The 50% isoline (black dotted) for the ozone concentration difference between the particle core and the near-surface bulk and the 63% (=1 – 1/e) isoline of $L_b^*$ (black dashed) remain near-constant throughout the simulation. They are from the beginning at the same level reached at the end of BC1, which reflects that both ozone and oleic can be regarded as well mixed in BC2 due to slow

reaction and rapid diffusion.

### 3.3 Base case 3: kinetic limitation by bulk diffusion

Base case 3 is based on base case 1 but the bulk diffusion coefficients are lower by five orders of magnitude ($D_{b,X}=10^{-10}\,cm^2\,s^{-1}$, $D_{b,Y}=10^{-15}\,cm^2\,s^{-1}$, Table 1), corresponding to characteristic diffusivities of amorphous (semi-)solid matrices (Bird et al., 2007; Swallen et al., 2007; Mikhailov et al., 2009).

As illustrated in Fig. 8a, the decay of oleic acid is very slow in BC3 because the low diffusivity effectively protects oleic acid in the particle bulk from oxidation. Within ~1 s the calculated ozone uptake coefficient drops from the initial value of $\sim 4\times10^{-3}$ to $\sim 2\times10^{-5}$, which is due to a rapid decrease of the oleic acid surface concentration from $\sim 10^{14}\,cm^{-2}$ to $\sim 10^{12}\,cm^{-2}$. After ~1 s the ozone surface concentration remains practically constant at $\sim 10^{12}\,cm^{-2}$ (adsorption equilibrium). The low levels of ozone uptake coefficient and oleic acid surface concentration are maintained by surface bulk exchange and decrease slowly as ozone increases and oleic acid decreases also in the near-surface bulk. In contrast to BC1, the bulk accommodation coefficient $\alpha_{b,X}$ ($\approx 2\times10^{-6}$) is much smaller than $\alpha_{s,X}$ and $\gamma_X$, reflecting the slow uptake of ozone into the particle bulk, which is limited by the kinetics of surface-bulk exchange and bulk diffusion.

Compared to KM-SUB, the simulated decay of oleic acid is faster and the ozone uptake coefficient is higher in K2-SUB, because the latter does not resolve bulk diffusion and the concentration profile of oleic acid. In fact, the diffusion coefficient of oleic acid ($D_{b,Y}$) does not appear in the equation for the reacto-diffusive flux (Eq. C1), which represents the effects of all bulk processes the resistor model approach.

Due to fast reaction and slow diffusion, both ozone and oleic acid exhibit steep concentration gradients near the surface, whereas the inner particle bulk remains nearly unchanged (Fig. 9). During the simulation period ozone penetrates only into the near-surface bulk, and thus the chemical consumption of oleic acid is also restricted to the near-surface bulk ($r/r_p>0.99$). Accordingly, the reacto-diffusive length is very small



(~0.1 nm; black solid line in Fig. 9a), and the 50% isoline (black dotted) for the ozone concentration difference between particle core and near-surface bulk as well as the 63% (=1 – 1/e) isoline of $L_b^*$ (black dashed) remain restricted to the near surface bulk ($r/r_p>0.99$). This is also reflected in Fig. 10, showing that the values of $L_b$ and $L_b^*$ are essentially zero except for $k=1$ (near-surface bulk layer).

### 3.4 Chemical half-life of oleic acid and atmospheric implications

We showed how the KM-SUB model can be used to interpret and analyze experimental data from laboratory studies in the previous sections. Laboratory studies are often carried out with high $O_3$ concentration to reduce the reaction time. Now we demonstrate how the results can be extrapolated to atmospheric conditions.

We estimated the chemical half-life ($t_{1/2}$) of pure oleic acid particles, when exposed to ambient $O_3$ mixing ratios (<150 ppb). The radii of oleic acid particles ($r_p$) were set to be 0.2 and 1.0 µm. The chemical half-life was defined as the time when number of oleic acid molecules was degraded to half of its initial value. The solid lines of Fig. 11 show the results of such calculations with BC1. At typical atmospheric $O_3$ mixing ratios of 30 ppb, $t_{1/2}$ was ~25 min for $r_p=0.2$ µm and ~130 min for $r_p=1.0$ µm. The chemical half-life depended strongly on particle radius (i.e. number of oleic acid molecules contained in the particle). In the typical polluted air with 100 ppb $O_3$, $t_{1/2}$ was shortened to ~8 min for $r_p=0.2$ µm and ~40 min for $r_p=1.0$ µm. The calculations were also made in BC2, which gave almost the same results for $r_p=0.2$ µm and gave ~20% smaller value for $r_p=1.0$ µm compared to BC1.

The ozonolysis reaction of oleic acid leads to an increased oxygen content and water uptake increases with longer ozone exposure (Asad et al., 2004). Although pure oleic acid is CCN-inactive, ozonolysis reaction can make particles CCN-active. The modeling results suggest that the transformation of oleic acid particles will occur in the timescale of ~1 h in the ambient atmosphere depending on the $O_3$ concentration and particle size. This is in excellent agreement with a 1.3 h lifetime worked out in Sect. 4.5 in King et al. (2009).

However, oleic acid is detected also in aged atmospheric aerosol particles (Rogge et al., 1991; Morris et al., 2002). The possible explanations are: reduced concentration of $O_3$ (and other photo-oxidants) in the particle bulk by (a) chemical reaction with other reactive species, self-reaction or catalytic decomposition or (b) slow mass transport because of low diffusion coefficients (semi-solid matrix, ultra-viscous, glassy, rubbery, and gel-like) due to oligomer formation and/or low temperature. To demonstrate this effect, the sensitivity studies were conducted with lower diffusion coefficients, which correspond to diffusivities characteristic for diffusion in solid or semi-solid matrices (Bird et al., 2007; Swallen et al., 2007; Mikhailov et al., 2009). The dotted line in Fig. 11 shows the calculation results reducing diffusion coefficients of $O_3$ and oleic acid of three orders of magnitudes ($D_{b,X}=10^{-8}\,cm^2\,s^{-1}$, $D_{b,Y}=10^{-13}\,cm^2\,s^{-1}$), resulting in ∼30% longer $t_{1/2}$ for both diameters. The dashed line shows the results using $D_{b,X}=10^{-10}\,cm^2\,s^{-1}$ and $D_{b,Y}=10^{-15}\,cm^2\,s^{-1}$, showing the big increase of $t_{1/2}$. $t_{1/2}$ was ∼170 min (∼3 h) for $r_p=0.2\,\mu m$ and ∼4100 min (∼2.8 d) for $r_p=1.0\,\mu m$, almost independent on $O_3$ mixing ratios.

## 4 Conclusions

We present a novel kinetic multi-layer model (KM-SUB) that explicitly resolves all steps of mass transport and chemical reaction at the surface and in the bulk of aerosol particles. It includes adsorption and desorption, surface reactions and surface-bulk exchange as well as bulk diffusion and reaction.

Unlike earlier models of aerosol chemistry (e.g. resistor model), the KM-SUB model approach does not require any simplifying assumptions about steady-state and mixing conditions. The temporal evolution of concentration profiles of volatile and non-volatile species in the particle bulk can be modeled along with surface concentrations and uptake coefficients.

In this study we explore and exemplify the effects of bulk diffusion on the rate of reactive gas uptake for a simple reference system, the ozonolysis of oleic acid particles, in



comparison to experimental data and earlier model studies. The effect of bulk diffusion on the rate of uptake and chemical reaction explored for a reference reaction (ozonolysis of oleic acid particles) with different sets of kinetic parameters (surface accommodation coefficients, diffusion coefficients, etc.) and particle size. The KM-SUB model was compared with the K2-SUB model and the partial differential equation method, which resulted in fairly good agreement. We show how the KM-SUB model can be used to interpret and analyze experimental data from laboratory studies, and how the results can be extrapolated to atmospheric conditions. For liquid oleic acid particles, the chemical half-life of oleic acid molecules with regard to oxidation by ozone is estimated to be ∼1 h. In (semi-)solid particles with low bulk diffusivity, however, the chemical half-life of can increase dramatically (up to hours and days). The results of sensitivity studies with different bulk diffusion coefficients confirm that the phase state of atmospheric particles is highly relevant for chemical transformation and aging (McNeill et al., 2007, 2008; Griffiths et al., 2009; Mikhailov et al., 2009).

Depending on the complexity of the investigated system, unlimited numbers of volatile and non-volatile species and chemical reactions can be added flexibly. Thus, the KM-SUB approach may serve as a basis for the development of a detailed master mechanism of aerosol chemistry and for the derivation of simplified but realistic parameterizations for large-scale atmospheric and climate models.

## Appendix A

### List of Symbols

| Symbol | Meaning | Unit |
|---|---|---|
| $\alpha_{b,X_i}$ | bulk accommodation coefficient of $X_i$ | |
| $\alpha_{s,0,X_i}$ | surface accommodation coefficient of $X_i$ on an adsorbate-free surface | |
| $\alpha_{s,X_i}$ | surface accommodation coefficient of $X_i$ | |
| $\delta$ | thickness of bulk layers | cm |
| $\delta_{X_i}$, $\delta_{Y_j}$ | effective molecular diameter of $X_i$ and $Y_j$ | cm |
| $\theta_s$ | sorption layer surface coverage | |
| $\sigma_{s,X_i}$ | molecular cross section of $X_i$ in the sorption layer | $cm^2$ |
| $\gamma_{X_i}$ | uptake coefficient of $X_i$ (normalized by gas kinetic flux of surface collisions) | |
| $\tau_{d,X_i}$ | desorption lifetime of $X_i$ | s |
| $\omega_{X_i}$ | mean thermal velocity of $X_i$ in the gas phase | $cm\,s^{-1}$ |
| $A(k)$ | outer surface area of bulk layer $k$ | $cm^2$ |
| $A_{ss}$ | surface area of particle (quasi-static layer) | |
| $C_{b,rd,X_i}$ | reacto-diffusive geometry correction factor for $X_i$ | |
| $C_{g,X_i}$ | gas phase diffusion correction factor for $X_i$ | |
| $J_{ads,X_i}$, $J_{des,X_i}$ | flux of adsorption and desorption of $X_i$ | $cm^{-2}\,s^{-1}$ |
| $J_{coll,X_i}$ | flux of surface collisions of $X_i$ | $cm^{-2}\,s^{-1}$ |
| $J_{b,rd,X_i}$ | reacto-diffusive flux of $X_i$ | $cm^{-2}\,s^{-1}$ |
| $J_{b,s,X_i}$, $J_{b,ss,Y_j}$ | flux of bulk-to-surface transport of $X_i$ (sorption layer) and $Y_j$ (quasi-static layer) | $cm^{-2}\,s^{-1}$ |
| $J_{s,b,X_i}$, $J_{ss,b,Y_j}$ | flux of surface-to-bulk transport of $X_i$ (sorption layer) and $Y_j$ (quasi-static layer) | $cm^{-1}\,s^{-1}$ |



| | | |
|---|---|---|
| $J_{bk,bk-1,X_i}$, $J_{bk,bk-1,Y_j}$ | flux of transport from bulk layer $k$ to bulk layer $k-1$ for $X_i$ and $Y_j$ | $cm^{-2}\,s^{-1}$ |
| $k_{b,b,X_i}$, $k_{b,b,Y_j}$ | rate coefficient (velocity) of bulk transport of $X_i$ and $Y_j$ | $cm\,s^{-1}$ |
| $k_{b,s,X_i}$ | rate coefficient (velocity) of bulk-to-surface transport of $X_i$ | $cm\,s^{-1}$ |
| $k_{BR,X_i,Y_j}$ | second-order rate coefficients for bulk reactions of $X_i$ with $Y_j$ | $cm^3\,s^{-1}$ |
| $k_{b,ss,Y_i}$ | rate coefficient (velocity) of bulk-to-surface transport of $Y_j$ | $cm\,s^{-1}$ |
| $k_{d,X_i}$ | first-order desorption rate coefficient of $X_i$ | $s^{-1}$ |
| $k_{s,b,X_i}$ | first-order rate coefficient for surface-to-bulk transport of $X_i$ | $s^{-1}$ |
| $k_{ss,b,Y_j}$ | first-order rate coefficients for surface-bulk transport of $Y_j$ | $s^{-1}$ |
| $k_{SLR,X_p,Y_q}$ | second-order rate coefficients for surface layer reactions of $X_p$ with $Y_q$ | $cm^2\,s^{-1}$ |
| $K_{sol,cc,X_i}$ | gas-particle partitioning coefficient of $X_i$ | |
| $l_{rd,X_i}$ | reacto-diffusive lenght oss rate of $X_i$ and $Y_j$ by reaction in the particle bulk | $cm^{-3}\,s^{-1}$ |
| $L_{b,X_i}$, $L_{b,Y_j}$ | loss rate of $X_i$ and $Y_j$ by reaction in the particle bulk | $cm^{-3}\,s^{-1}$ |
| $L_{bk,X_i}$, $L_{bk,Y_j}$ | loss rate of $X_i$ and $Y_j$ by reaction in bulk layer $k$ | $cm^{-3}\,s^{-1}$ |
| $L_{s,X_i}$, $L_{ss,Y_j}$ | loss rate of $X_i$ and $Y_j$ by surface layer reaction | $cm^{-2}\,s^{-1}$ |

| | | |
|---|---|---|
| $L^*_{b,X_i}$, $L^*_{b,Y_j}$ | absolute loss rate of $X_i$ and $Y_j$ by reaction in the particle bulk | $s^{-1}$ |
| $L^*_{bk,X_i}$, $L^*_{bk,Y_j}$ | absolute loss rate of $X_i$ and $Y_j$ by reaction in bulk layer $k$ | $s^{-1}$ |
| $L^*_{s,X_i}$, $L^*_{ss,Y_j}$ | absolute loss rate of $X_i$ and $Y_j$ by surface layer reaction | $s^{-1}$ |
| $n$ | number of bulk layers | |
| $P_{b,X_i}$, $P_{b,Y_j}$ | production rate of $X_i$ and $Y_j$ by reaction in the particle bulk | $cm^{-3}\,s^{-1}$ |
| $P_{bk,X_i}$, $P_{bk,Y_j}$ | production rate of $X_i$ and $Y_j$ by reaction in bulk layer $k$ | $cm^{-3}\,s^{-1}$ |
| $P_{s,X_i}$, $P_{ss,Y_j}$ | production rate of $X_i$ and $Y_j$ by surface layer reaction | $cm^{-2}\,s^{-1}$ |
| $r_b$ | particle bulk radius | cm |
| $r_p$ | particle radius | cm |
| $[X_i]_g$ | gas phase number concentration of $X_i$ | $cm^{-3}$ |
| $[X_i]_{gs}$ | near-surface gas phase number concentration of $X_i$ | $cm^{-3}$ |
| $[X_i]_s$ | surface number concentration of $X_i$ (sorption layer) | $cm^{-2}$ |
| $[Y_j]_{ss}$ | surface number concentration of $Y_j$ (quasi-static layer) | $cm^{-2}$ |
| $[X_i]_{bk}$, $[Y_j]_{bk}$ | Bulk number concentration of $X_i$ and $Y_j$ in the bulk layer $k$ | $cm^{-3}$ |
| $V_b$ | volume of particle bulk | |
| $V(k)$ | volume of bulk layer $k$ | $cm^{-3}$ |



## Appendix B

### Partial differential equation model (PDE)

Smith et al. (2003) demonstrated that the diffusion and reaction in the bulk can be described by the following partial differential equations:

$$\frac{\partial [X]_b}{\partial t} = \frac{D_{b,X}}{r^2}\frac{\partial}{\partial r}\left(r^2\frac{\partial [X]_b}{\partial r}\right) - k_{BR,X,Y}[X]_b[Y]_b \quad \text{(B1)}$$

$$\frac{\partial [Y]_b}{\partial t} = \frac{D_{b,Y}}{r^2}\frac{\partial}{\partial r}\left(r^2\frac{\partial [Y]_b}{\partial r}\right) - k_{BR,X,Y}[X]_b[Y]_b \quad \text{(B2)}$$

where X=$O_3$ and Y=oleic acid. The first term describes diffusion based on the Fick's law and the second term describes chemical reaction in the bulk. Note that this partial differential equation (PDE) method can only simulate the processes in the bulk and not coupled with surface processes. In solving these PDE equations, several assumptions are required as boundary conditions (Smith et al., 2003): 1) the concentration of the near-surface bulk is fixed over time, 2) the flux of X at the core is zero ($\partial[X]_b/\partial r|_{r=0}=0$), 3) the flux of Y at both near-surface bulk and core is zero ($\partial[X]_b/\partial r|_{r=r_p}=\partial[X]_b/\partial r|_{r=0}=0$). PDE model simulations were performed by numerically solving the partial differential equations with Matlab software (PDEPE solver).

We investigate large particles with a radius of 1.0 µm as investigated by Smith et al. (2003), and we compare the KM-SUB results ($n$=200) to the results of the PDE model. The gas phase ozone concentration was set to $[X]_g=[X]_{gs}=7.0\times10^{13}$ $cm^{-3}$ (corresponding to 2.8 ppm at 1013 hPa and 298 K). The initial surface and bulk concentrations of ozone (X) were set to $[X]_{s,0}=[X]_{bk,0}=0$, and the initial surface and bulk concentrations of oleic acid (Y) were set to $[Y]_{ss,0}=9.7\times10^{13}$ $cm^{-2}$ and $[Y]_{ss,0}=1.2\times10^{21}$ $cm^{-3}$, respectively. The kinetic parameters used are based on base case 1 summarized in Table 1 with the second-order surface reaction rate coefficient ($k_{SLR,X,Y}$) of zero. Unlike

KM-SUB, the PDE model depends on the assumption of a fixed ozone concentration in the near surface bulk. Smith et al. (2003) had assumed solubility saturation according to Henry's law. In case of fast reaction, however, chemical loss leads to a substantial decrease and lower value of the actual ozone concentration. For comparability, the concentration of ozone in the near-surface bulk of the PDE model was set to a value of $5.0\times10^{13}$ cm$^{-3}$, which is similar to the value calculated by KM-SUB.

Figure A1 shows the concentration profiles of ozone (top) and oleic acid (bottom) obtained by simulations with KM-SUB (left) and with the PDE model (right). The diffusion of $O_3$ into the bulk was very slow due to the large particle diameter, so that there was a large concentration gradient of $O_3$. The concentration of $O_3$ at the core remains small ($<10^3$ cm$^{-3}$) over the reaction time considered. Oleic acid showed also a concentration gradient, which was due to the $O_3$ concentration gradient and a slow diffusion coefficient of oleic acid ($D_{b,Y}=10^{-10}$ cm$^2$ s$^{-1}$). If a larger $D_{b,Y}$ of $10^{-7}$ cm$^2$ s$^{-1}$ was used in the simulation, the concentration of oleic acid was homogeneous throughout the bulk, which was consistent with the results reported by Smith et al. (2003).

The KM-SUB and PDE methods yield very similar results, but the concentration gradients for both $O_3$ and oleic acid were slightly steeper in the PDE model. A possible reason for the difference may be that the PDE model requires the assumption of a fixed ozone concentration in the near surface bulk and zero flux values at the surface and at center of the particles as specified above (boundary conditions). Another possible reason for deviations is the estimation of bulk transport velocities ($k_{b,b}$). If we assume $k_{b,b} = D_b/\delta$ instead of Eqs. (35) and (36), the KM-SUB results become nearly identical to the PDE results. Note that varying the number of layers in the KM-SUB model made practically no difference.



## Appendix C

### Kinetic double-layer model (K2-SUB)

A kinetic double-layer of surface and bulk chemistry (K2-SUB) was developed by Pfrang et al. (2009). K2-SUB uses one layer for bulk, therefore concentration profiles in the bulk is not obtained. The diffusion and reaction in the bulk is considered by the reacto-diffusive flux ($J_{b,rd}$) (Danckwerts, 1951; Hanson, 1997; Pöschl et al., 2007). The loss rate of oleic acid in the bulk can be described as follows (Pfrang et al., 2009), which is based on the resistor model formulation (Hanson, 1997):

$$L_{b,Y} = J_{b,rd,X}\frac{A_{ss}}{V_b} = C_{b,rd,X}\sqrt{k_{BR,X,Y}[Y]_b D_{b,X}}[X]_{bs}\frac{A_{ss}}{V_b} \quad \text{(C1)}$$

where $A_{ss}$ and $V_b$ is the surface area and volume of bulk particle. $C_{b,rd,X}$ is the reacto-diffusive geometry correction factor (conversion from planar to spherical geometry) (Pöschl et al., 2007). $C_{b,rd,X}$ is a function of particle radius ($r_p$) and the reacto-diffusive length $l_{rd,X}$, which can be regarded as the distance from the surface up to which the chemical reaction proceeds effectively (Finlayson-Pitts and Pitts, 2000; Pöschl et al., 2007):

$$C_{b,rd,X} = \coth\left(\frac{r_p}{l_{rd,X}}\right) - \frac{l_{rd,X}}{r_p} \quad \text{(C2)}$$

$$l_{rd,X} = \sqrt{D_{b,X}/(k_{BR,X,Y}[Y]_b)} \quad \text{(C3)}$$

K2-SUB presented by Pfrang et al. (2009) assumed the steady-state condition of $O_3$ in surface and bulk. K2-SUB was modified by removing these assumptions by including the gas-surface interaction fluxes (adsorption ($J_{ads,X}$), desorption ($J_{des,X}$) and surface layer reaction ($L_{s,X}$ and $L_{ss,X}$)) in the differential equations (X=$O_3$, Y=oleic acid). The differential equations below can be solved using Matlab solver.

$$d[X]_s/dt = J_{ads,X} - J_{des,X} - L_{s,X} - J_{s,b,X} + J_{b,s,X} \quad \text{(C4)}$$

$$d[Y]_{ss}/dt = J_{b,ss,Y} - J_{ss,b,Y} - L_{ss,Y} \quad \text{(C5)}$$

$$d[X]_b/dt = (J_{s,b,X} - J_{b,s,X} - J_{b,rd,X})A_{ss}/V_b \quad \text{(C6)}$$

$$d[Y]_b/dt = (J_{ss,b,Y} - J_{b,ss,Y} - J_{b,rd,X})A_{ss}/V_b \quad \text{(C7)}$$

*Acknowledgements.* This work was funded by the Max Planck Society (MPG) and the European integrated project on cloud climate and air quality interactions (No 036833-2 EUCAARI). MS is supported by the Max Planck Graduate Center (MPGC) and the Ministry of Education, Culture, Sports, Science and Technology – Japan (MEXT). CP wishes to thank the Royal Society (grant VO080001) and the NERC (grant NE/G000883/1). We acknowledge M. Ammann for stimulating discussions.

The service charges for this open access publication
have been covered by the Max Planck Society.

## References

Ammann, M., Kalberer, M., Jost, D. T., Tobler, L., Rossler, E., Piguet, D., Gaggeler, H. W., and Baltensperger, U.: Heterogeneous production of nitrous acid on soot in polluted air masses, Nature, 395, 157–160, 1998.

Ammann, M. and Pöschl, U.: Kinetic model framework for aerosol and cloud surface chemistry and gas-particle interactions – Part 2: Exemplary practical applications and numerical simulations, Atmos. Chem. Phys., 7, 6025–6045, 2007, http://www.atmos-chem-phys.net/7/6025/2007/.

Andreae, M. O. and Rosenfeld, D.: Aerosol-cloud-precipitation interactions. Part 1. The nature and sources of cloud-active aerosols, Earth-Sci. Rev., 89, 13–41, 2008.

Anttila, T., Kiendler-Scharr, A., Tillmann, R., and Mentel, T. F.: On the reactive uptake of gaseous compounds by organic-coated aqueous aerosols: theoretical analysis and application to the heterogeneous hydrolysis of $N_2O_5$, J. Phys. Chem. A, 110, 10435–10443, 2006.

Asad, A., Mmereki, B. T., and Donaldson, D. J.: Enhanced uptake of water by oxidatively processed oleic acid, Atmos. Chem. Phys., 4, 2083–2089, 2004, http://www.atmos-chem-phys.net/4/2083/2004/.



Atkins, P. W.: Physical Chemistry, Oxford University Press, Oxford, 1998.

Bird, R. B., Stewart, W. E., and Lightfoot, E. N.: Transport Phenomena (2nd Ed.), John Wiley & Sons, Inc., New York, 2007.

Danckwerts, P. V.: Absorption by simultaneous diffusion and chemical reaction into particles of various shapes and into falling drops, T. Faraday Soc., 47, 1014–1023, 1951.

Finlayson-Pitts, B. J. and Pitts, J. N. (eds.): Chemistry of the Upper and Lower Atmosphere, Academic Press, San Diego, California, 2000.

Fuzzi, S., Andreae, M. O., Huebert, B. J., Kulmala, M., Bond, T. C., Boy, M., Doherty, S. J., Guenther, A., Kanakidou, M., Kawamura, K., Kerminen, V.-M., Lohmann, U., Russell, L. M., and Pöschl, U.: Critical assessment of the current state of scientific knowledge, terminology, and research needs concerning the role of organic aerosols in the atmosphere, climate, and global change, Atmos. Chem. Phys., 6, 2017–2038, 2006, http://www.atmos-chem-phys.net/6/2017/2006/.

Griffiths, P. T., Badger, C. L., Cox, R. A., Folkers, M., Henk, H. H., and Mentel, T. F.: Reactive uptake of $N_2O_5$ by aerosols containing dicarboxylic acids. Effect of particle phase, composition, and nitrate content, J. Phys. Chem. A, 113, 5082–5090, 2009.

Hallquist, M., Wenger, J. C., Baltensperger, U., Rudich, Y., Simpson, D., Claeys, M., Dommen, J., Donahue, N. M., George, C., Goldstein, A. H., Hamilton, J. F., Herrmann, H., Hoffmann, T., Iinuma, Y., Jang, M., Jenkin, M. E., Jimenez, J. L., Kiendler-Scharr, A., Maenhaut, W., McFiggans, G., Mentel, Th. F., Monod, A., Prévôt, A. S. H., Seinfeld, J. H., Surratt, J. D., Szmigielski, R., and Wildt, J.: The formation, properties and impact of secondary organic aerosol: current and emerging issues, Atmos. Chem. Phys., 9, 5155–5235, 2009, http://www.atmos-chem-phys.net/9/5155/2009/.

Hanson, D. R.: Surface-specific reactions on liquids, J. Phys. Chem. B, 101, 4998–5001, 1997.

Hearn, J. D., Lovett, A. J., and Smith, G. D.: Ozonolysis of oleic acid particles: evidence for a surface reaction and secondary reactions involving Criegee intermediates, Phys. Chem. Chem. Phys., 7, 501–511, 2005.

Hearn, J. D. and Smith, G. A.: Ozonolysis of mixed oleic acid/n-docosane particles: the roles of phase, morphology, and metastable states, J. Phys. Chem. A, 111, 11059–11065, 2007.

Kanakidou, M., Seinfeld, J. H., Pandis, S. N., Barnes, I., Dentener, F. J., Facchini, M. C., Van Dingenen, R., Ervens, B., Nenes, A., Nielsen, C. J., Swietlicki, E., Putaud, J. P., Balkanski, Y., Fuzzi, S., Horth, J., Moortgat, G. K., Winterhalter, R., Myhre, C. E. L., Tsigaridis, K., Vignati, E., Stephanou, E. G., and Wilson, J.: Organic aerosol and global climate modelling:

a review, Atmos. Chem. Phys., 5, 1053–1123, 2005, http://www.atmos-chem-phys.net/5/1053/2005/.
Katrib, Y., Biskos, G., Buseck, P. R., Davidovits, P., Jayne, J. T., Mochida, M., Wise, M. E., Worsnop, D. R., and Martin, S. T.: Ozonolysis of mixed oleic-acid/stearic-acid particles: reaction kinetics and chemical morphology, J. Phys. Chem. A, 109, 10910–10919, 2005.
Katrib, Y., Martin, S. T., Hung, H. M., Rudich, Y., Zhang, H. Z., Slowik, J. G., Davidovits, P., Jayne, J. T., and Worsnop, D. R.: Products and mechanisms of ozone reactions with oleic acid for aerosol particles having core-shell morphologies, J. Phys. Chem. A, 108, 6686–6695, 2004.
King, M. D., Rennie, A. R., Thompson, K. C., Fisher, F. N., Dong, C. C., Thomas, R. K., Pfrang, C., and Hughes, A. V.: Oxidation of oleic acid at the air-water interface and its potential effects on cloud critical supersaturations, Phys. Chem. Chem. Phys., 11, 7699–7707, 2009.
King, M. D., Thompson, K. C., and Ward, A. D.: Laser tweezers Raman study of optically trapped aerosol droplets of seawater and oleic acid reacting with ozone: implications for cloud-droplet properties, J. Am. Chem. Soc., 126, 16710–16711, 2004.
King, M. D., Thompson, K. C., Ward, A. D., Pfrang, C., and Hughes, B. R.: Oxidation of biogenic and water-soluble compounds in aqueous and organic aerosol droplets by ozone: a kinetic and product analysis approach using laser Raman tweezers, Faraday Discuss., 137, 173–192, 2008.
McNeill, V. F., Wolfe, G. M., and Thornton, J. A.: The oxidation of oleate in submicron aqueous salt aerosols: evidence of a surface process, J. Phys. Chem. A, 111, 1073–1083, 2007.
McNeill, V. F., Yatavelli, R. L. N., Thornton, J. A., Stipe, C. B., and Landgrebe, O.: Heterogeneous OH oxidation of palmitic acid in single component and internally mixed aerosol particles: vaporization and the role of particle phase, Atmos. Chem. Phys., 8, 5465–5476, 2008, http://www.atmos-chem-phys.net/8/5465/2008/.
Mikhailov, E., Vlasenko, S., Martin, S. T., Koop, T., and Pöschl, U.: Amorphous and crystalline aerosol particles interacting with water vapor: conceptual framework and experimental evidence for restructuring, phase transitions and kinetic limitations, Atmos. Chem. Phys., 9, 9491–9522, 2009, http://www.atmos-chem-phys.net/9/9491/2009/.
Moise, T. and Rudich, Y.: Reactive uptake of ozone by proxies for organic aerosols: surface



versus bulk processes, J. Geophys. Res.-Atmos., 105, 14667–14676, 2000.
Moise, T. and Rudich, Y.: Reactive uptake of ozone by aerosol-associated unsaturated fatty acids: kinetics, mechanism, and products, J. Phys. Chem. A, 106, 6469–6476, 2002.
Morris, J. W., Davidovits, P., Jayne, J. T., Jimenez, J. L., Shi, Q., Kolb, C. E., Worsnop, D. R., Barney, W. S., and Cass, G.: Kinetics of submicron oleic acid aerosols with ozone: a novel aerosol mass spectrometric technique, Geophys. Res. Lett., 29(9), 1357, doi:10.1029/2002gl014692, 2002.
Pfrang, C., Shiraiwa, M., and Pöschl, U.: Coupling aerosol surface and bulk chemistry with a kinetic double layer model (K2-SUB): oxidation of oleic acid by ozone, Atmos. Chem. Phys. Discuss., 9, 26969–27019, 2009, http://www.atmos-chem-phys-discuss.net/9/26969/2009/.
Pöschl, U.: Formation and decomposition of hazardous chemical components contained in atmospheric aerosol particles, J. Aerosol Med., 15, 203–212, 2002.
Pöschl, U.: Atmospheric aerosols: composition, transformation, climate and health effects, Angew. Chem. Int. Edit., 44, 7520–7540, 2005.
Pöschl, U., Rudich, Y., and Ammann, M.: Kinetic model framework for aerosol and cloud surface chemistry and gas-particle interactions – Part 1: General equations, parameters, and terminology, Atmos. Chem. Phys., 7, 5989–6023, 2007, http://www.atmos-chem-phys.net/7/5989/2007/.
Rincon, A. G., Guzman, M. I., Hoffmann, M. R., and Colussi, A. J.: Optical absorptivity versus molecular composition of model organic aerosol matter, J. Phys. Chem. A, 113, 10512–10520, 2009.
Rogge, W. F., Hildemann, L. M., Mazurek, M. A., Cass, G. R., and Simonelt, B. R. T.: Sources of fine organic aerosol: 1. Charbroilers and meat cooking operations, Environ. Sci. Technol., 25, 1112–1125, 1991.
Rudich, Y.: Laboratory perspectives on the chemical transformations of organic matter in atmospheric particles, Chem. Rev., 103, 5097–5124, 2003.
Schwartz, S. E. and Freiberg, J. E.: Mass-transport limitation to the rate of reaction of gases in liquid droplets – application to oxidation of $SO_2$ in aqueous-solutions, Atmos. Environ., 15, 1129–1144, 1981.
Seinfeld, J. H. and Pandis, S. N.: Atmospheric Chemistry and Physics – From Air Pollution to Climate Change, John Wiley & Sons, Inc., New York, 1998.
Shiraiwa, M., Garland, R. M., and Pöschl, U.: Kinetic double-layer model of aerosol surface

chemistry and gas-particle interactions (K2-SURF): Degradation of polycyclic aromatic hydrocarbons exposed to $O_3$, $NO_2$, $H_2O$, OH and $NO_3$, Atmos. Chem. Phys., 9, 9571–9586, 2009,
http://www.atmos-chem-phys.net/9/9571/2009/.

Smith, G. D., Woods, E., Baer, T., and Miller, R. E.: Aerosol uptake described by numerical solution of the diffusion – reaction equations in the particle, J. Phys. Chem. A, 107, 9582–9587, 2003.

Springmann, M., Knopf, D. A., and Riemer, N.: Detailed heterogeneous chemistry in an urban plume box model: reversible co-adsorption of O3, NO2, and H2O on soot coated with benzo[a]pyrene, Atmos. Chem. Phys., 9, 7461–7479, 2009,
http://www.atmos-chem-phys.net/9/7461/2009/.

Swallen, S. F., Kearns, K. L., Mapes, M. K., Kim, Y. S., McMahon, R. J., Ediger, M. D., Wu, T., Yu, L., and Satija, S.: Organic glasses with exceptional thermodynamic and kinetic stability, Science, 315, 353–356, 2007.

Vesna, O., Sjogren, S., Weingartner, E., Samburova, V., Kalberer, M., Gggeler, H. W., and Ammann, M.: Changes of fatty acid aerosol hygroscopicity induced by ozonolysis under humid conditions, Atmos. Chem. Phys., 8, 4683–4690, 2008,
http://www.atmos-chem-phys.net/8/4683/2008/.

Wiedensohler, A., Cheng, Y. F., Nowak, A., Wehner, B., Achtert, P., Berghof, M., Birmili, W., Wu, Z. J., Hu, M., Zhu, T., Takegawa, N., Kita, K., Kondo, Y., Lou, S. R., Hofzumahaus, A., Holland, F., Wahner, A., Gunthe, S. S., Rose, D., Su, H., and Pöschl, U.: Rapid aerosol particle growth and increase of cloud condensation nucleus activity by secondary aerosol formation and condensation: A case study for regional air pollution in Northeastern China, J. Geophys. Res.-Atmos., 114, D00G08, doi:10.1029/2008JD010884, 2009.

Worsnop, D. R., Morris, J. W., Shi, Q., Davidovits, P., and Kolb, C. E.: A chemical kinetic model for reactive transformations of aerosol particles, Geophys. Res. Lett., 29, 57–1-4, doi:10.1029/2002GL015542, 2002.

Zahardis, J. and Petrucci, G. A.: The oleic acid-ozone heterogeneous reaction system: products, kinetics, secondary chemistry, and atmospheric implications of a model system a review, Atmos. Chem. Phys., 7, 1237–1274, 2007,
http://www.atmos-chem-phys.net/7/1237/2007/.

Ziemann, P. J.: Aerosol products, mechanisms, and kinetics of heterogeneous reactions of ozone with oleic acid in pure and mixed particles, Faraday Discuss., 130, 469–490, 2005.



**Table 1.** Kinetic parameters for the interaction of ozone (X) and oleic acid (Y) in different model scenarios (base cases 1–3).

| Parameter | Base case 1 | Base case 2 | Base case 3 |
|---|---|---|---|
| $\alpha_{s,0,X}$ | $4.2\times10^{-4}$ | $8.5\times10^{-4}$ | $4.2\times10^{-4}$ |
| $\tau_{d,X}$ (s) | 0.01 | 0.001 | 0.01 |
| $D_{b,X}$ ($cm^2\,s^{-1}$) | $10^{-5}$ | $10^{-5}$ | $10^{-10}$ |
| $D_{b,Y}$ ($cm^2\,s^{-1}$) | $10^{-10}$ | $10^{-10}$ | $10^{-15}$ |
| $k_{SLR,X,Y}$ ($cm^2\,s^{-1}$) | $6.0\times10^{-12}$ | $6.0\times10^{-12}$ | $6.0\times10^{-12}$ |
| $k_{BR,X,Y}$ ($cm^3\,s^{-1}$) | $1.7\times10^{-15}$ | $5.0\times10^{-17}$ | $1.7\times10^{-15}$ |

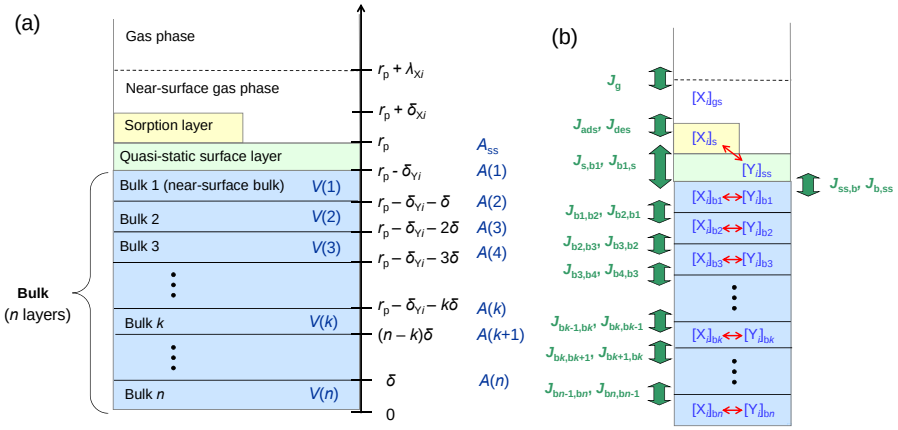


**Fig. 1.** Kinetic multi-layer model (KM-SUB): **(a)** model compartments and layers with corresponding distances from particle center ($r_p \pm x$), surface areas ($A$) and volumes ($V$); $\lambda_{X_i}$ is the mean free path of $X_i$ in the gas phase; $\delta_{X_i}$ and $\delta_{Y_i}$ are the thicknesses of sorption and quasi-static bulk layers; $\delta$ is the bulk layer thickness. **(b)** Transport fluxes (green arrows) and chemical reactions (red arrows).



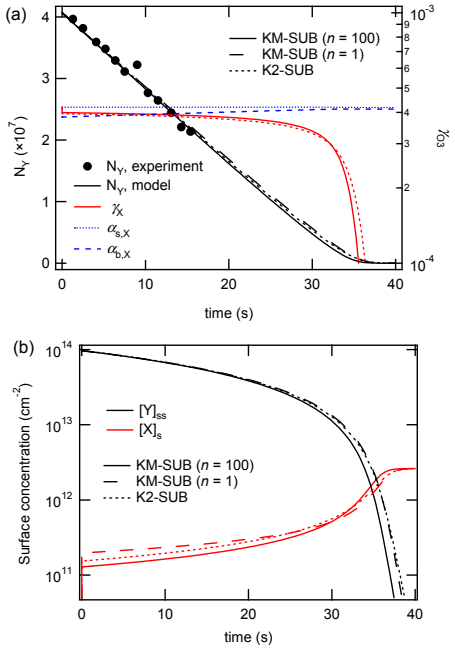


**Fig. 2.** Temporal evolution of model base case 1 in KM-SUB with $n = 1$ (dashed lines) and $n = 100$ (solid lines), and in K2-SUB (dotted lines). **(a)** Experimental data (black symbols; Ziemann, 2005) and model results for the total number of oleic acid molecules ($N_Y$, black line) and for the uptake coefficient of ozone ($\gamma_{X_i}$, red line), surface accommodation coefficient ($\alpha_{s,X}$, blue dotted line), and bulk accommodation coefficient ($\alpha_{b,X}$, blue dashed line). **(b)** Surface concentrations of oleic acid (black line) and ozone (red line).

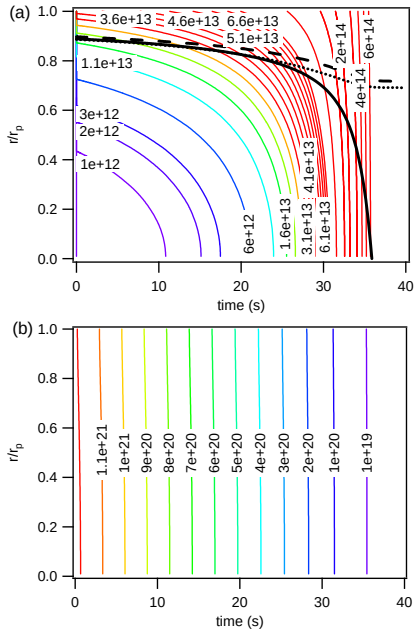


**Fig. 3.** Temporal evolution of bulk concentration profiles for model base case 1 for **(a)** ozone and **(b)** oleic acid (KM-SUB with $n$=100). The $y$-axis indicates the radial distance from the particle center ($r$) normalized by the particle radius, ranging from the particle core ($r/r_p=\delta/r_p\approx0$) to the near-surface bulk ($r/r_p=1$). The colored lines are isopleths of bulk concentration with labeled in units of cm$^{-3}$ (blue=low, red=high). The black solid line represents the reacto-diffusive length for ozone normalized by the particle radius ($1-l_{rd}/r_p$). The black dotted line represents the 50% isoline for the concentration difference between the particle core and the near-surface bulk, and the black dashed line shows 63% isoline of $L_b^*$.

317

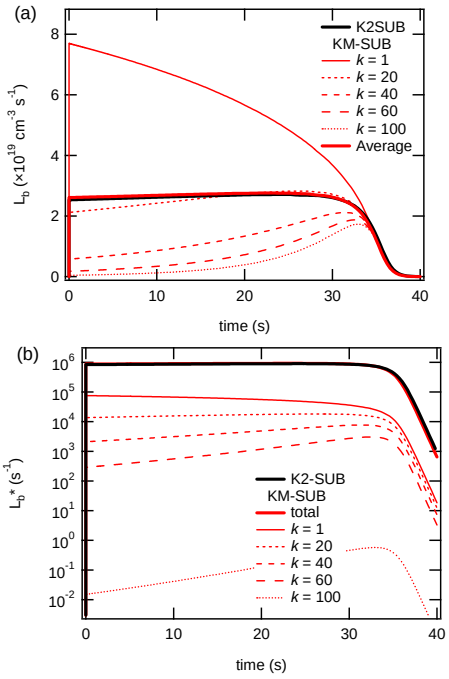


**Fig. 4. (a)** Loss rate ($L_b$) and **(b)** absolute loss rate ($L_{bk}^*$) of oleic acid in the bulk calculated by KM-SUB in the bulk 1 (near-surface bulk), 20, 40, 60, and 100 (core) in BC1. $L_b$ calculated by K2-SUB and volume average $L_b$ ($=L_b^*/V_b$) calculated by KM-SUB are shown in panel **(a)**. Total absolute los rate ($L_b^*$) calculated by KM-SUB and K2-SUB are also shown in panel **(b)**.

318

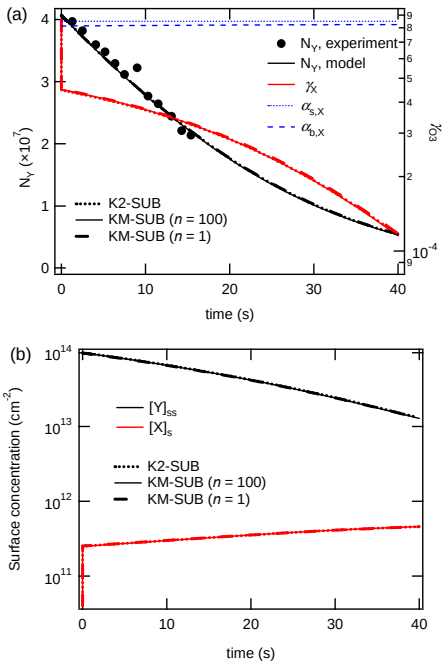


**Fig. 5.** Temporal evolution of model base case 2 in KM-SUB with $n = 1$ (dashed lines) and $n = 100$ (solid lines), and in K2-SUB (dotted lines). **(a)** Experimental data (black symbols; Ziemann, 2005) and model results for the total number of oleic acid molecules ($N_Y$, black line) and for the uptake coefficient of ozone ($\gamma_X$, red line), surface accommodation coefficient ($\alpha_{s,X}$, blue dotted line), and bulk accommodation coefficient ($\alpha_{b,X}$, blue dashed line). **(b)** Surface concentrations of oleic acid (black line) and ozone (red line).

319

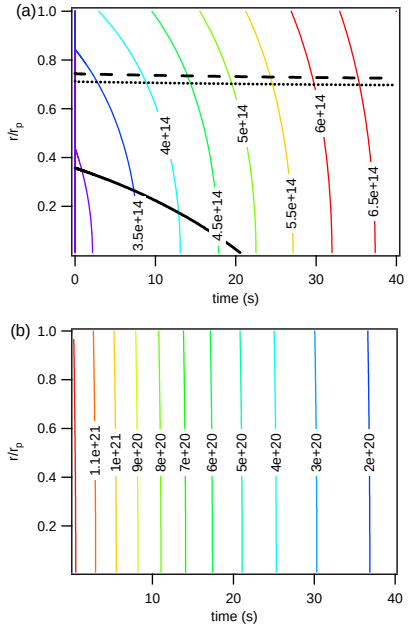


**Fig. 6.** Temporal evolution of bulk concentration profiles for model base case 1 for **(a)** ozone and **(b)** oleic acid (KM-SUB with $n$=100). The $y$-axis indicates the radial distance from the particle center ($r$) normalized by the particle radius, ranging from the particle core ($r/r_p=\delta/r_p\approx0$) to the near-surface bulk ($r/r_p=1$). The colored lines are isopleths of bulk concentration with labeled in units of cm$^{-3}$ (blue=low, red=high). The black solid line represents the reacto-diffusive length for ozone normalized by the particle radius ($1-l_{rd}/r_p$). The black dotted line represents the 50% isoline for the concentration difference between the particle core and the near-surface bulk, and the black dashed line shows 63% isoline of $L_b^*$.

320

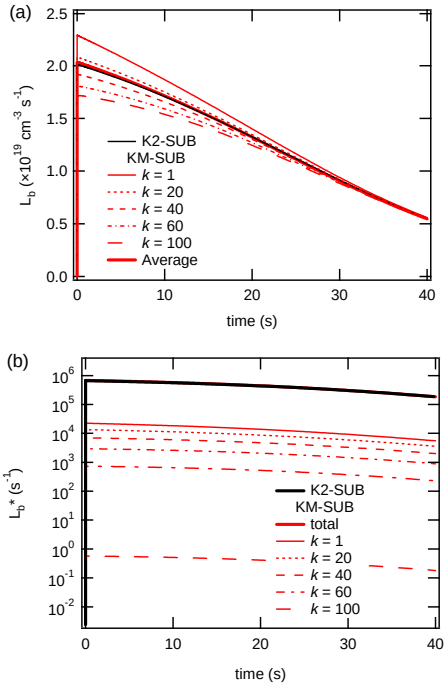


**Fig. 7. (a)** Loss rate ($L_b$) and **(b)** absolute loss rate ($L^*_{bk}$) of oleic acid in the bulk calculated by KM-SUB in the bulk 1 (near-surface bulk), 20, 40, 60, and 100 (core) in BC2. $L_b$ calculated by K2-SUB and volume average $L_b$ ($=L^*_b/V_b$) calculated by KM-SUB are shown in panel (a). Total absolute los rate ($L^*_b$) calculated by KM-SUB and K2-SUB are also shown in panel (b).



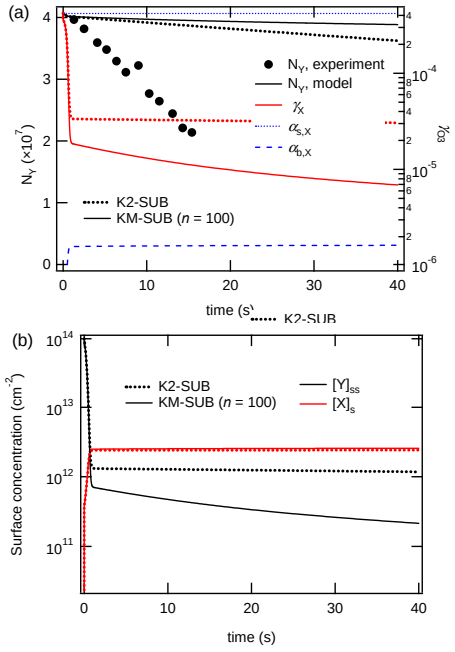


**Fig. 8.** Temporal evolution of model base case 3 with KM-SUB ($n$=100). **(a)** Experimental data (black symbols; Ziemann, 2005) and model results for the total number of oleic acid molecules ($N_Y$, black line) and for the uptake coefficient of ozone ($\gamma_X$, red line), surface accommodation coefficient ($\alpha_{s,X}$, blue dotted line), and bulk accommodation coefficient ($\alpha_{b,X}$, blue dashed line). **(b)** Surface concentrations of oleic acid (black line) and ozone (red line).

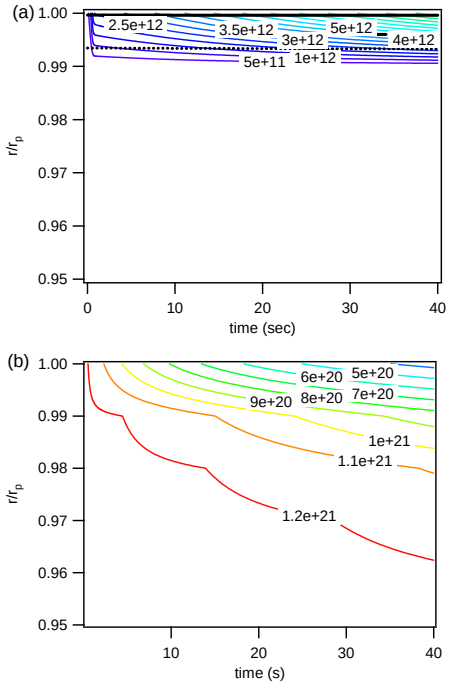


**Fig. 9.** Temporal evolution of bulk concentration profiles for model base case 3 for **(a)** ozone and **(b)** oleic acid (KM-SUB with $n$=100). The $y$-axis indicates the radial distance from the particle center ($r$) normalized by the particle radius, ranging from $r/r_p$=0.95 to the near-surface bulk ($r/r_p$=1). The colored lines are isopleths of bulk concentration with labeled in units of cm$^{-3}$ (blue=low, red=high). The black dotted line represents the 50% isoline for the concentration difference between the particle core and the near-surface bulk, and the black dashed line shows 63% isoline of $L_b^*$.

323

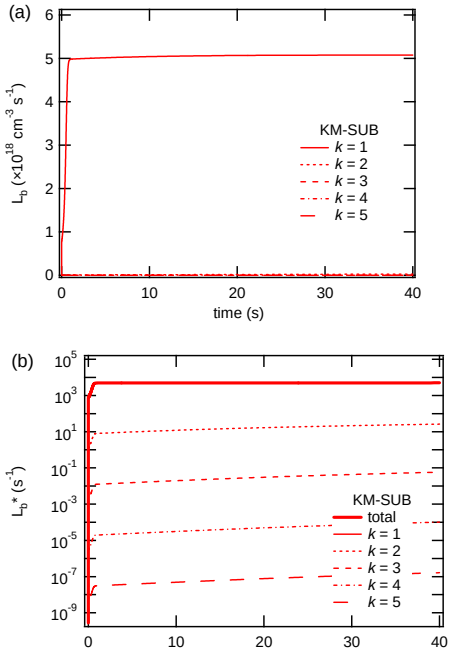


**Fig. 10. (a)** Loss rate ($L_b$) and **(b)** absolute loss rate ($L_{bk}^*$) of oleic acid in the bulk calculated by KM-SUB in the bulk 1 (near-surface bulk), 20, 40, 60, and 100 (core) in BC2. Total absolute los rate ($L_b^*$) are also shown.

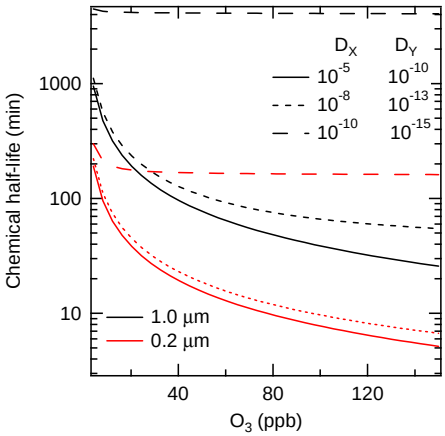


**Fig. 11.** Chemical half-life (min) of pure oleic acid particles with particle radius of 1.0 (black) and 0.2 µm (red) as a function of gas phase $O_3$ concentration. The diffusion coefficients are $D_X=10^{-5}$ cm$^2$ s$^{-1}$, $D_Y=10^{-10}$ cm$^2$ s$^{-1}$ (solid line, BC1), $D_X=10^{-8}$ cm$^2$ s$^{-1}$, $D_Y=10^{-13}$ cm$^2$ s$^{-1}$ (dotted line), and $D_X=10^{-10}$ cm$^2$ s$^{-1}$, $D_Y=10^{-15}$ cm$^2$ s$^{-1}$ (dashed line, BC3).



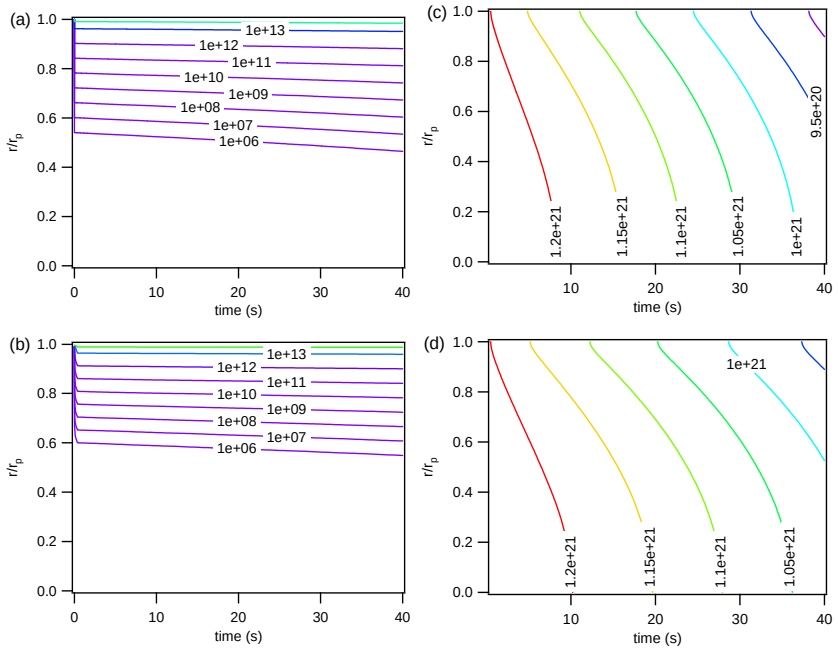


**Fig. A1.** Temporal evolution of bulk concentration profiles for ozone by **(a)** KM-SUB and **(b)** PDE method and for oleic acid by **(c)** KM-SUB and **(d)** PDE method. The $y$-axis indicates the radial distance from the particle center ($r$) normalized by the particle radius, ranging from the particle core ($r/r_p \approx 0$) to the near-surface bulk ($r/r_p=1$). The colored lines are isopleths of bulk concentration with labeled in units of cm$^{-3}$ (blue=low, red=high).